Revista Cubana de Meteorología

Revista Cubana de Meteorología, Vol. 30, No. sp, 2024, ISSN: 2664-0880

Artículo Original

Influence of atmospheric and oceanic indexes on interannual precipitation in San Ramon, Costa Rica

Influencia de índices atmosféricos y océanos en la precipitación interanual en San Ramón, Costa Rica

https://cu-id.com/2377/v30nspe10

Marvin E. Quesada*

Catedrático, Universidad de Costa Rica

ABSTRACT: The interannual climatic variability of precipitation in San Ramón (El Estero stream micro-basin) and its relationship with indexes of the ONI (Oceanic Niño Index), MEIv2 (Multivariate ENSO Index, version 2). CLLJ (Caribbean Low Level Jet Index), the NAO (North Atlantic Oscillation Index), and the SOI (Southern Oscillation Index). To calculate the interannual variation of precipitation, the mathematical analysis program Geogebra in its version 4 and the interquartile range (IQR) were used. Confidence intervals were established to observe the different intensities of ENSO, and precipitation was correlated with the different oceanic-atmospheric indices, showing a negative relationship in four of them and a positive relationship in only one. The NAO index shows a very low regression. With the ONI, the relationship with ENSO episodes was established, showing some relationship during La Niña (cold phase), producing above-average rainfall in the area under study. While during the El Niño event (warm phase) there have been decreases in precipitation.

***Keywords*:** Climate variability, ENSO, Geogebra, correlation, oceanic and atmospheric indices.

RESUMEN: Se analiza la variabilidad climática interanual de la precipitación en San Ramón (microcuenca quebrada El Estero) y su relación con los índices del ONI (Oceanic Niño Index), MEIv2 (Multivariate ENSO Index, version 2), CLLJI (Caribbean Low Level Jet Index), el NAO (North Atlantic Oscillation Index), y el SOI (Southern Oscillation Index). Para calcular la variación interanual de la precipitación se usó el programa de análisis matemático Geogebra en su versión 4 y el rango intercuartílico (RIC). Se establecieron intervalos de confianza para observar las distintas intensidades del ENOS, y se correlacionó la precipitación con los distintos índices oceánico- atmosféricos, visualizándose una relación negativa en cuatro de ellos y positiva en sólo uno. El índice NAO muestra una regresión muy baja. Con el ONI, se estableció la relación con los episodios del ENOS mostrando alguna relación durante La Niña (fase fría), produciéndose precipitaciones superiores al promedio en la zona en estudio. Mientras que durante el evento El Niño (fase cálida) se han producido mermas en la precipitación.

Palabras clave: Variabilidad climática, ENOS, Geogebra, correlación, índices oceánicos y atmosféricos.

1. INTRODUCTION

Interannual variability of precipitation describes the degree of consistency in year-over- year precipitation totals: higher variability equates to greater irregularity of annual totals about the annual mean, which brings precipitation extremes (Alfaro et al, 2012). Some periods are dry, other exceeds rain, which reflects that the precipitation patterns are shifting globally due to climate variability. Those changes are driven by decrease or increase in moisture availability in the environment, rising or decreasing temperature in the Pacific and Atlantic Oceans, in continental region and shifts in atmospheric circulation patterns, such a poleward expansion of the Hadley cell (Polade et al., 2014; Tao et al. 2016).

Quesada and Marsik (2014) consider that changes in sea surface temperatures are due to low or high atmospheric pressures in both oceans. These can occur in different ways, whether one ocean has high atmospheric pressure and the other low or both have low atmospheric pressures, the latter case is currently happening (IMN, 2023). These changes in atmospheric pressures can lead to the ENSO, El Niño (Warm Phase) or the La Niña (Cold Phase) in the equatorial Pacific Ocean. Therefore, intense rainfall associated events like La Niña and some atmospheric-oceanic conditions could cause a severe flood in cities, which resulted in high losses of infrastructures estimated costs of several million dollars (Boers et al., 2014; Frame, et al., 2015).

*Autor para correspondencia: Marvin E. Quesada. E-mail: marvin.quesada@ucr.ac.cr

Received: 15/12/2023

Accepted: 07/02/2024

Conflicto de intereses: El autor declara no tener conflictos de interés

Furthermore, extreme weather events are episodes that some years ago occur very rarely, while lately those are happened very often with serious consequences on the environment and human health (Fowler, et al, 2021). It is evidence that global warming has altered the water cycle, which has led to change in the magnitude, frequency, and probability of extreme rainfall around the world (Bengtsson et al, 2014; Du et al, 2014; Mei et al, 2018). Among the climatic parameters, precipitation plays a vital role in the tropics, being the main climate element changing agricultural production, due to extreme droughts or floods (Alfaro, 2000; Vuille et al., 2012). During the last decades, studies focused on documenting the climate variability along Costa Rica have provided valuable information to understand current and past dynamics of the climatic system (Amador et al., 2006; Quesada et al., 2012; Alfaro et al, 2012; Amador, 2016).

The mountain and valleys ecosystems of the tropical pacific region of Costa Rica is highly sensitive to changes in rainfall patterns, due to the different altitudinal floors (Quesada, 2019). Recent studies have contributed to better understand the effects of the climate variations on mountain ecosystems (Sheldon, 2019). Several events of heavy rains have led to landslides in the upper mountains and downstream inundations (Varun et al, 2006), some of which severely affected the cities like San Ramon.

In this context, extensive research taking into consideration rainfall and atmospheric- oceanic indexes represents an essential tool to properly characterize the climate fluctuations on interannual rainfall over San Ramon, which presents a river that cross the main city and causes floods during the rainy season. This research aims to investigate the possible influence of existing climate indices in adjacent oceans on interannual rainfall in San Ramon. At the same time, this study has the particularity that it studies a region that, despite being located on the Pacific slope and the existence of a mountain range that crosses the country from Northwest to Southeast, there is an intermontane depression that allows the incursion of winds, air masses loaded with moisture from the Caribbean sector to the Pacific of Costa Rica.

2. MATERIALS AND METHODS

2.1. Study Region and Climate

The study area encompasses the El Estero micro basin located in the San Ramon County, which is a tropical region with a defined dry season since December to March and a rainy season between May to October, with two transitional months April and November. The onset of the wet season in the El Estero micro basin in San Ramon typically occurs between September and October with deep convection covers most Pacific range of Costa Rica, where this micro basin is located. Fig.1.

The regional intensification of the air circulation is coming from the West due to the Equatorial Western winds, which transports considerable moisture from the Pacific Ocean. Those winds flow at the same time of the Intertropical Convergence Zone (ITCZ) which characterizes seasonal rainfall variability over San Ramon region. When the ITZC migrates to the Southward, and the dry season is accompanied by

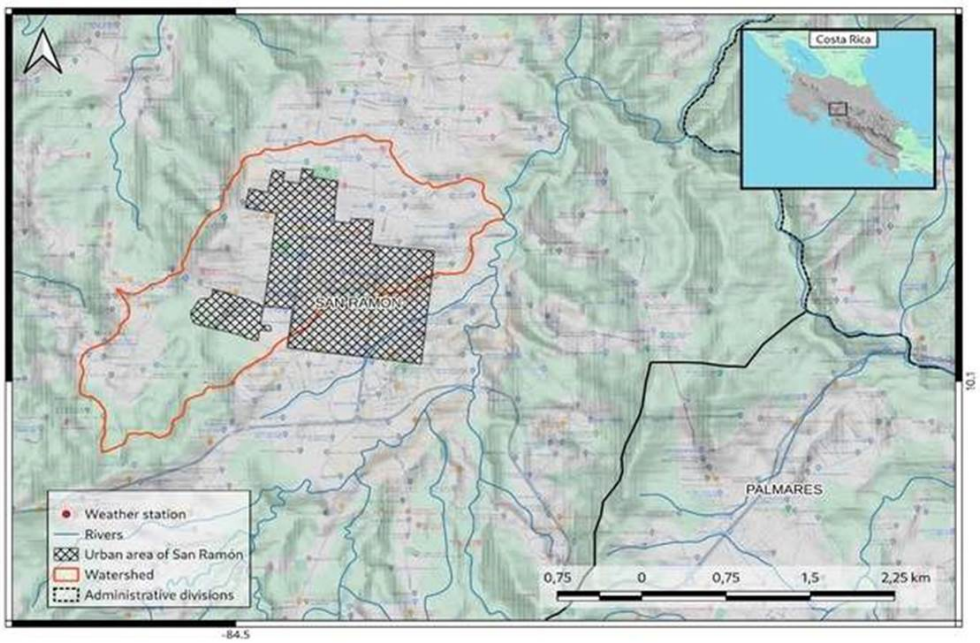

Source. Own elaborated by using a topographical map. Naranjo. 1: 50000.

Figura 1. Relative location of the Study area, San Ramon.

Table 1. Description of the significance of the Mann test - Kendall

SIGNIFICANCE	YMBOLOGY	Z
No Trend	ST	0
Significant Trend Increasing	TSC	> + 1,96
Significant downward trend	TSD	< - 1,96
Increasing non-significant trend	TNSC	< + 1,96
Decreasing non-significant trend	TNSD	> - 1,96

Source: Alves *et al.* 2015

decreased rainfall in the San Ramon to almost disappear, even though sometimes rains.

Precipitation increases on the slopes with eastern exposure, which in turn produces "rain shadow" effect leeward, creating drier environments in the intermountain valleys. On wetter slopes, rainfall varies from 780 to 2900 and sometimes more than 3700 mm/ year.

2.2. Datasets

There used the longest and most complete monthly precipitation records from a network station compiled by the Electrical National Institute (ICE), and it is compiled by another stations that it is in the Sede Occidente, University of Costa Rica. It will be called San Ramon meteorological station, for more facility. This station has a long-term record (1940-2020), that is an excellent record in a rural region of Costa Rica. This makes it possible to investigate the possible influence of the adjacent oceans and seas and the interannual behavior of precipitation in the region where San Ramón is located.

2.3. Trend Analysis

2.3.1. Mann-Kendall test

The time series for each extreme rainfall index was determined using the non-parametric Mann-Kendall statistical test to evaluate the temporal trends analysis. It has been widely employed for rainfall trend analysis (Endo et all, 2000; Doyle et all, 2012; Cerón ,2021) In this study, the Mann-Kendall was performed at a significance level of 0.05. The statistical programming language R This function is described by Mclead (2022) in the official documentation of the R project.

According to Muñoz (2008), the data set must first be ordered, in this case the entire precipitation record for San Ramón from 1950 to 2020. The data must be sorted in such a way as to comply:

$$\left(x_j - x_k\right)conj > k \quad (1)$$

From this, a matrix is constructed where the sign of the consecutive sums is determined, as follows:

$$sign\left(x_j - x_k\right) = \begin{Bmatrix} 1if\left(x_j - x_k\right) > 0 \\ 0if\left(x_j - x_k\right) = 0 \\ -1if\left(x_j - x_k\right) < 0 \end{Bmatrix} \quad (2)$$

$$S = \sum_{k=1}^{n-1}\sum_{j=k+1}^{n} sign\left(x_j - x_k\right) \quad (3)$$

Where:

$$sign\left(x\right) = \begin{Bmatrix} +1ifx > 0 \\ 0ifx = 0 \\ -1ifx < 0 \end{Bmatrix} \quad (4)$$

It is assumed that S must represent an approximately normal distribution. S indicates the possible existence of trends in the data, if the data is non-zero, H0 (null hypothesis) can be accepted or rejected.

Subsequently, the variance is determined using the formula:

$$Var\left[S\right] = \frac{1}{18}(n(n-1)(2n+5)) \quad (5)$$

where **n** is the population size or total amount of data, which for precipitation from January 1950 to December 2020 is 852 months of records.

Considering the sign of S, the value of Z (significance) is determined by the following criteria:

$$Z = 0\begin{Bmatrix} \frac{(S-1)}{Var[S]^{\frac{1}{2}}} ifS > 0 \\ 0ifS = 0 \\ \frac{(S+1)}{Var[S]^{1/2}} ifS < 0 \end{Bmatrix} \quad (6)$$

Z evaluates the existence of a statistically significant trend, positive values indicate an increase in the trend, a negative value shows a decrease. "To test any trend, increasing or decreasing, for a α level of significance, the null hypothesis is rejected when the absolute value of Z is greater than Z1 - α/2." (Alencar & Silva, 2017, p. 301). Normally the α value is 0.05 or 5% significant.

Finally, the hypothesis of interest is evaluated considering the value of 1.96 as the critical Z, according to the following table.

$$\tau = \frac{S}{D} \quad (7)$$

Where:

S: is the standard deviation

D: is calculated by:

$$D = \frac{\left(\frac{1}{2}n(n-1) - \frac{1}{2}\sum_{j=1}^{P} t_j\left(t_j - 1\right)\right)^{1/2}}{\left(\frac{1}{2}n(n-1)\right)^{1/2}} \quad (8)$$

Mann Kendall Trend Test (M- K test) is a non-parametric test which has been widely used for analysis of rainfall trends in different parts of the world, and we use this test to find trends of rainfall,

rain days and extreme indices for the minor season. In the M-K test the null hypothesis assumes there is no trend and it's tested against the alternative hypothesis (there is trend). The Mann Kendell Statistics S, the Variance of S V (S) and the standard test statistics Z are stated mathematically by Equation 1 represents the statistic of the Mann-Kendall test.

High positive values of Mann Kendell Statistics S, Variance of S V(S) and standard test statistics Z indicates an increasing trend whilst high negative values show decreasing trends. Sen's Slope Estimator Technique is a non-parametric method of estimating the magnitude of a trend based on the method of least squares and we apply this method to find magnitudes of trends in the minor season.

2.4. Interannual change in precipitation

By means of the mathematical analysis program Geogebra in its version 4, the correlation graphs were elaborated, as well as the calculation of the statistics. As stated on its website, "GeoGebra is a dynamic mathematical software for all educational levels that brings together geometry, algebra, spreadsheets, graphs, statistics, and calculus in a single engine" (Mendenhall et al., 2010).

Through the spreadsheet section, the variables to be analyzed are introduced: precipitation and a climate index, then these are compared through a bivariate analysis, automatically providing a scatter or correlation graph between both variables, as well as the statistics. It allows you to generate a line of best fit according to a linear function, or other polynomials of second or more degrees, exponential functions, logarithmic functions. In this case, it was worked only with linear functions to generate the best fit line for the correlation.

To create the wisker-box graphs, the free software version 4 Geogebra was used. Wisker- box plots summarize the behavior of the ordered data set, identifying important values such as the average, minimums, and maximums, first and third quartiles. The area of the box is defined by the interquartile range (IQR), which is calculated as follows:

$$RIC = Q_3 - Q_1 \quad (9)$$

Q1 corresponds to 25% of the data set, the mean (towards the center of the box) indicates 50% of the data. Q3 shows the position of 75% of the data set. The "whiskers" (the straight lines with endings) extend about 1.5 times the interquartile range (IQR) from Q1 and Q3. Outside the box and the "whiskers" are the outliers, which correspond to the values in the dataset closest to:

$$Outliers = \begin{Bmatrix} Q_1 - 1.5RIC \\ Q_3 + 1.5RIC \end{Bmatrix} \quad (10)$$

The wisker-box chart can be represented both vertically and horizontally and is a visual summary of the main statistics.

The figures were plotted using Geogebra version 4. Using the spreadsheet section, the data of the precipitation variable (either monthly cumulative or annual cumulative) is imported and analyzed using a univariate analysis. The program displays the statistics automatically and allows you to generate a histogram with the desired number of classes, which can be specified manually. Sturges' rule, proposed by Herbert Sturges in 1926 to determine the number of classes, was used to construct histograms (Hyndman, 1995). This is calculated as follows:

$$k = 1 + log_2 n \quad (11)$$

Where:

k is the number of classes

n is the size of the data sample (81 in the case of interannual precipitation)

2.4.1. ENSO Temperature Anomalies

Based on the ONI value for the corresponding period, temperature anomalies were calculated, considering that there are El Niño conditions when the ONI index is greater than 0.5 °C, La Niña conditions when the ONI is less than -0.5 °C. So: *Anomaly of El Niño = ONI + 0.5 Anomaly of La Niña = ONI - 0.5*

To qualify the anomalies, the IMN (2018) was considered, which is summarized in the following table:

Table 2. ENSO Intensity Rating

Intensity	Temperature anomaly
Very weak	Less than 0.3 °C
Weak to moderate	From 0.3 °C to 0.8 °C
Strong	From 0.81 °C to 1.2 °C
Very strong	Up to 1.2 °C

Source. Own adaptation based on IMN (2018).

2.5. Pearson's R

This is one of the most widely used correlation measures. As indicated by many statistical books, such as that of Mendenhall et al. (2010), its specific name is Pearson's product moment correlation coefficient, which is used to linearly compare the relationship between the variances (covariances) of two variables. Its mathematical formula is given by:

$$r = \frac{S_{xy}}{S_x S_y} = \frac{S_{xy}}{S_{xx} S_{yy}}; for -1 \leq r \leq +1$$

where $\boldsymbol{S}$ is the variance, $\boldsymbol{x}$ and $\boldsymbol{y}$ are respective variables. In the coefficient, the respective crosses are made between the variances and covariances of the two variables, resulting in a value of between -1 and +1. When this value is close to 0 it implies a very low linear correlation, consequently, values close to +1 imply a high positive correlation (both variables grow in the same direction), while values close to - 1 imply a high correlation but in a negative way (both variables grow in different directions).

"In general, when a sample of n individuals or experimental units is selected and two variables are measured in each individual or unit, so that both variables are random, the correlation coefficient r is the appropriate measure of linearity to use in this situation." (Mendenhall et al., 2010). It is also important to consider that there is a direct relationship between the calculation of the slope of a regression line b in a linear function and Pearson's r, so that the sign of r is always equal to the sign of the slope of b (in a function of the *form* $\hat{y} = a + bx$). So the following relationships are given:

1. When r = 0, the slope is b = 0, and there is no linear correlation between *x* and *y*.
2. If r is positive, *b* is also positive, and there is a positive linear relationship between *x*
3. and *y*.
4. If r is negative, *b* is also negative, and there is a negative linear relationship between *x* and *y*.

It is from this relationship that scatter plots or correlation plots are constructed. The figure below illustrates the idea of linear correlation.

2.6. R² or coefficient of determination

As Mendenhall et al. (2010) indicate, one way to measure the strength of the relationship between a response variable "y" and *the predictor variable* "x" is *to calculate the coefficient of determination, i.e., the proportion of the total variation that is explained by the regression of* y *into* x. It is used to measure the degree of certainty of Pearson's linear regression model r. It corresponds essentially to the square of Pearson's correlation coefficient r, as deduced from the following formula.

$$\frac{SSR}{SSTOTAL} = \frac{(S_{xy})^2}{S_{xx}S_{yy}} = \left(\frac{S_{xy}}{\sqrt{S_{xx}S_{yy}}}\right)^2 = r^2 \quad (13)$$

where SSR is the sum of squares for the regression and Total SS is the total variation.

The r² can be interpreted as "the percentage reduction in the total variation in the experiment obtained by using the regression line $\hat{y} = a + bx$, rather than ignoring *x* and using the sample mean $\hat{y}$ y to predict the response variable *y*." (Mendenhall et al., 2010).

Therefore, it is common to interpret the value of r² as a percentage rather than the decimal; being, for example, a value of 0.752 interpreted as the 75.2% success rate of the linear model, which is very high. Lower values such as 0.106 would indicate a certainty of 10.6%, which is a low predictive ability using linear regression.

3. RESULTS

3.1. Mann-Kendall test

The non-parametric Mann-Kendall test was performed on the values of the annually accumulated precipitation. According to the results of the Mann-Kendall test, precipitation in the El Estero micro-basin showed significant increasing and decreasing trends. The results are closely related to the El Niño and La Niña years. The results can be seen in the following graph. As can be seen there are years that present very low values such as 1956, 1972, 1982 and 2015, among others.

While other years show high rainfall values such as 1954, 1973, 1974, 1998 and 2012 among others. The value of Z is significant increasing (TSC) at 0.257. This result indicates that in the time series from 1940 to 2020 there is a trend of increase in rainfall in the micro- basin.

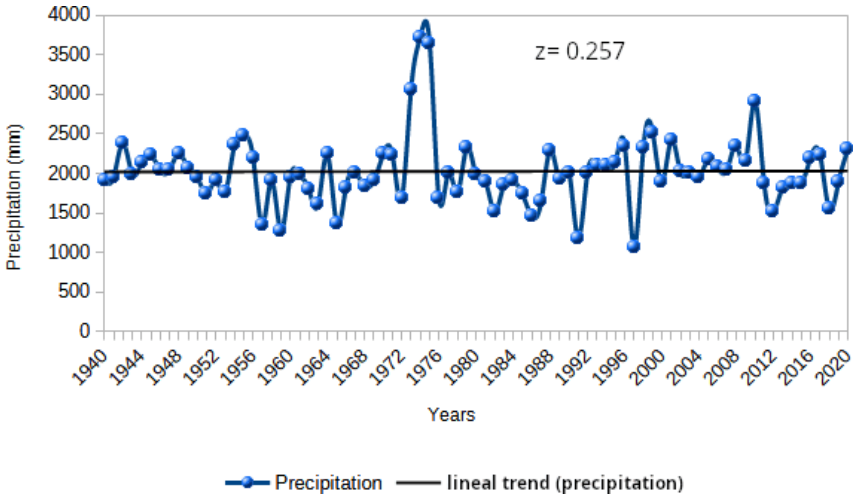

Source. Own elaborated by using rainfall data of San Ramon station.

Figura 2. Mann Kendall distribution of interannual rainfall in San Ramon

The value of S is non-zero, so that the null hypothesis H0 can be accepted or rejected. Since the tau value is greater than zero, the null hypothesis H0 can be rejected, and the possibility of an alternative hypothesis validated. It is true that Z < +1.96, indicating that there is an increasing non-significant trend in the precipitation data. Behavior must be explained by an alternative hypothesis.

3.2. Precipitation analysis and descriptive statistics

The figure below shows the general behavior of precipitation accumulated interannually during the recording period. As can be seen, the period from 1973 to 1975 presents a very intense uptick in the amount of precipitation, related to an intense Cold phase of ENSO. Also, around 1991 and 1997 there were the greatest precipitation deficits, related to warm event.

The dark straight line in the figure above is indicating the average value for the entire data record: 2023 mm of precipitation. With the record of accumulated rainfall interannual from 1940 to 2020, the statistics that describe the behavior of the data can be calculated, these are shown in the following table.

Table 3. Statistics of accumulated year-on-year precipitation from 1940 to 2020.

Parameter	Value
N	81
Median	1994.4
Minimal	1070
Maximum	3726
Average	2023.69
Standard Deviation (S)	428.04
Moda	1911.8
First Quartile	1832.15
Third Quartile	2230.59
Variance (Σ)	425.39

Source. Author's elaboration based on records from San Ramón station, 2023.

The high value of the standard deviation of the sample (s) and the variance (σ) indicate that the data have a high dispersion and variability over time. The great variability between the minimum and maximum values can be noted, since even for the annual accumulated values there is a difference of more than double between these values, between extremely rainy years, such as 1974, and extremely dry years, such as 1997.

To construct a histogram, Sturges' rule was applied: $k = 1 + log^2(81) = k = 7.34$. It was determined that the classes (k) should be around 7.34, it was decided to define them as 8 classes so that it would be an even number. The following table shows the frequency distribution prior to the construction of the histogram.

Table 4. Class intervals according to interannual variation in precipitation

Interval	Relative frequency
1070-1402	5
1403-1734	8
1735-2066	37
2067-2398	24
2399-2730	3
2731-3062	1
3063-3394	1
3395-3726	2

Source. Own elaboration based on precipitation records from the San Ramón Meteorological Station.

The following histogram of 8 classes shows the distribution of rainfall for the annual cumulative values from 1940 to 2020. It can be seen how the distribution of the data expands to the right with respect to a normal symmetric distribution or Gaussian bell, which indicates that the data are asymmetric and biased to the left. Therefore, the arithmetic mean is higher than the median (mean = 2023 > median = 1994), which is indeed true as shown in Table 2 above. In this case, the median value is a better indicator of the center of the data than the value of the average.

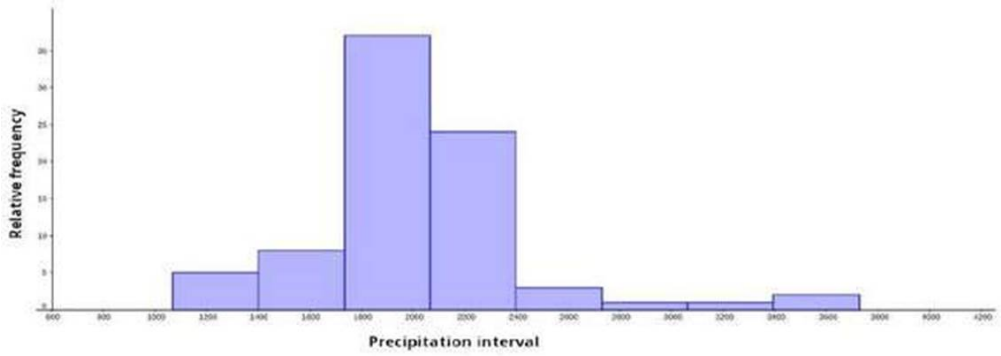

Source. Own elaboration based on rainfall records from the San Ramon meteorological station.

Figura 4. Relative frequency according to interannual variation in precipitation

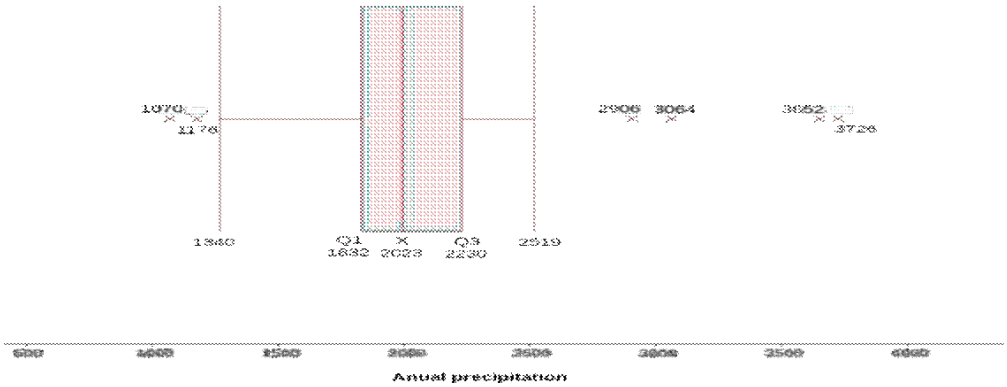

Source. Prepared by the author based on the San Ramón weather station, 2023.

Figure 5. Wisker-box diagram of interannual precipitation, 1940-2020

The following wisker-box graph shows the behavior of precipitation data. The clustering trend around the average value (the area of the box) can be seen, as well as the extreme values that go beyond the limits of the "whiskers", which are indicative of abnormally high or low rainfall and are associated with ENSO events.

There are some clearly outliers, outside the area of the box and the "whiskers", these are the first two and the last four of the data set ordered in ascending order: 1070 (minimum value and corresponding to precipitation in 1997, there was a period where El Niño affected with a deficit of rainfall in San Ramón), 1176 (1991), and the maximum values of 2906 (2010), 3064 (1973), 3652 (1975) and 3726 (maximum value corresponding to 1974). All these years correspond with intense La Niña events.

3.3. Influence of ENSO

The effects of ENSO in Costa Rica are well known, causing rainfall deficits when a warm phase arises and an increase when it corresponds to a cold phase, this for the Pacific slope and the central valley. Table 4 below shows a classification of ENSO cycles from December 1949 to June 2022. For temperature anomalies, the ONI value was considered.

It can be seen that the most intense El Niño event in terms of the maximum temperature of the ocean was the one of the period 2014-2016 with 2.14 °C in the value of the ONI, an anomaly of 2.14, had a more intense temperature peak than the El Niño of 1997, However, the latter is historically remembered as the one that caused the greatest affectation, It can be seen in the table that it coincided precisely with the rainy season of 1997. The Oceanic Niño Index (ONI) was used, which measures surface water temperature anomalies in the tropical Pacific, in zone 3-4.

The most intense La Niña corresponds to the years 1973-1974, which is followed by another strong La Niña in 1977-1978, which can be considered a second stage of the previous one, which would not only be the most intense La Niña due to the difference in temperature, but also because of its duration (15+18 = 33 months). Other Las Niñas of strong intensity due to their temperature anomaly are those of the years: 1988-1989, 1998-2001, 2007-2008 and 2010-2011.

The El Niño phase, the one in the years 1986-1988 is the longest since 1950 to the present, with 18 months. The longest lasting La Niña was that of 1998-2001, with 32 months active. In general, it is more common to find warm phases with a more marked temperature difference, compared to cold phases of ENSO,

The behavior of precipitation, in most of the Pacific slope of Costa Rica, is closely related to the variation of the trade flow, the westerly winds of the equatorial Pacific (Western equatorials), the position of the ITCZ; in addition to more local factors such as the position of the El Estero micro-basin with respect to their location, which gives it a mainly pacific regime, although the influences of the climatic regime of the Northern slope are not ruled out, since it sometimes rains during the early mornings, due to the incursion of air masses loaded with humidity that manage to pass through the depression of the Bajo Tapezco.

In addition to these climatic modifying factors, an important relationship with the behavior of ENSO can be seen through the Oceanic Niño Index (ONI) calculated by NOAA for zone 3-4 of the tropical Pacific. To do this, a correlation analysis should be used. The Pacific Slope of Costa Rican and temperature in the Pacific Ocean have an inverse behavior. The warmer the Pacific Ocean tends to rain less, the cooler the water tends to rain excessively. But to get a better idea, the following table 6 was prepared to reflect the most notorious relationships between rainfall and ENSO phases for the case of San Ramón.

If the result was greater than 12, the average was calculated by dividing the total number of months by 12. This result is divided by the sum of months, to adjust them to a period of 1 year. Under this classification the El Niños that have reduced rainfall the most in the area are those of the periods: 1965-1966, 1982-1983, 1991-1992 and 1997-1998, the latter showing the greatest reductions, with a

Table 5. Classification of ENSO cycles according to duration and intensity, 1950-2022

El Niño Events (Warm Phase)						La Niña Events (Cold Phase)					
Begin	**End**	**Duration**	**Max. Value ONI ºC**	**Anomaly**	**Intensity of anomaly**	**Begin**	**End**	**Duration**	**Min. Value ONI ºC**	**Anomaly**	**Intensity of anomaly**
May 1951	Jan 1952	9 months	1.15	0.65	Weak to moderate	Dec 1949	Feb 1950	3 months	-1.53	-1.03	Strong
Feb 1953	Jan 1954	12 months	0.84	0.34	Weak to moderate	Nov 1950	Feb 1951	4 months	-0.82	-0.32	Weak a moderate
Apr 1957	Jul 1959	16 months	1.81	1.31	Very strong	May 1954	Agu 1956	28 months	-1.67	-1.17	Strong
Jun 1963	Feb 1964	9 months	1.37	0.87	Strong	May 1964	Jan 1965	9 months	-0,82	-0.32	Weak a moderate
Jun 1965	Abr 1966	11 months	1.98	1.48	Very strong	Ene 1968	Mar 1968	3 months	-0.74	-0.24	Very weak
Oct 1968	May 1969	8 months	1.13	0.63	Weak to moderate	Jul 1970	Jan 1972	19 months	-1.38	-0.88	Strong
Aug 1969	Jan 1970	6 months	0.86	0.36	Weak to moderate	May 1973	Jul 1974	15 months	-2.03	-1.53	Very strong
May 1972	Mar 1973	11 months	2.12	1.62	Very strong	Oct 1974	Mar 1976	18 months	-1.65	-1.15	Strong
Sep 1976	Feb 1977	6 months	0.86	0.36	Weak to moderate	Oct 1983	Jan 1984	4 months	-1.0	-0.5	Weak a moderate
Sep 1977	Jan 1978	6 months	0.81	0.31	Weak to moderate	Oct 1984	Jun 1985	9 months	-1.14	-0.64	Weak a moderate
Nov 1979	Jan 1980	3 months	0.64	0.14	Very weak	May 1988	May 1989	13 months	-1.85	-1.35	Very strong
May 1982	Jun 1983	14 months	2.23	1.73	Very strong	Aug 1995	Mar 1996	8 months	-1.5	-1.0	Strong
Sep 1986	Feb 1988	18 months	1.70	1.2	Strong	Jul 1998	Feb 2001	32 months	-1.66	-1.16	Strong
Jun 1991	Jun 1992	13 months	1.71	1.21	Very strong	Nov 2005	Mar 2006	5 months	-0.85	-0.35	Weak a moderate
Sep 1994	Mar 1995	7 months	1.09	0.59	Weak to moderate	Jul 2007	Jun 2008	12 months	-1.64	-1.14	Strong
May 1997	Abr 1998	12 months	2.40	1.9	Very strong	Nov 2008	Mar 2009	5 months	-0,85	-0.35	Weak a moderate
Jun 2002	Feb 2003	9 months	1.31	0.81	Strong	Jun 2010	May 2011	12 months	-1.64	-1.14	Strong
Aug 2004	Feb 2005	7 months	0.7	0.2	Very weak	Aug 2011	Mar 2012	8 months	-1.09	-0.59	Weak a moderate
Sep 2006	Jan 2007	5 months	0.94	0.44	Weak to moderate	Ago 2016	Dec 2016	5 months	-0.69	-0.19	Very weak
Aug 2009	Mar 2010	8 months	1.56	1.06	Strong	Oct 2017	Abr 2018	7 months	-0.97	-0.47	Weak a moderate
Nov 2014	Jan 2016	3 months	0.66	0.16	Very weak	Aug 2020	Mar 2021	9 months	-1.27	-0.77	Weak a moderate
Mar 2015	Abr 2016	14 months	2.64	2.14	Very strong	Sep 2021	Jan 2023	17 months	-1.06	-0.56	Weak a moderate
Oct 2018	May 2019	8 months	0.90	0.4	Very weak						
Nov 2019	Jan 2020	3 months	0.55	0.05	Very weak						

Source. Author' elaboration based on NOAA (September 30, 2023).

Revista Cubana de Meteorología, Vol. 30, No. sp, 2024, ISSN: 2664-0880, https://cu-id.com/2377/v30nspe10

Table 6. ENSO Phases per periods and intensities.

ENSO Phase (Intensity)	Period	Duration	Extreme anomaly in temp. Oceanic (°C)	Precipitation Average of the period* (mm)	Difference from average total precipitation (2023 mm)	Level of Apparent Influence
Cold (strong)	**1954-1956**	**28 months**	**-1,17**	**2554**	**520**	High
Warm (very strong)	1957-1959	**23 months**	1,31	1690	-344	Medium
Warm (very strong)	**1965-1966**	**11 months**	**1,48**	**1398**	**-638**	Very high
Warm (very strong)	1972-1973	10 months	1,62	1642	-393	Medium
Cold (very strong)	**1973-1976**	**23 months**	**-1,53**	**3397**	**1363**	Extreme
Warm (very strong)	**1982-1983**	**14 months**	**1,73**	**1449**	**-585**	High
Warm (strong)	1986-1988	17 months	1,2	1748	-286	Medium
Cold (very strong)	1988-1989	13 months	-1,35	2369	335	Medium
Warm (very strong)	**1991-1992**	**13 months**	**1,21**	**1349**	**-685**	Very high
Warm (very strong)	**1997-1998**	**12 months**	**1,9**	**1102**	**-933**	Extreme
Cold (strong)	**1998-2001**	**32 months**	**-1,16**	**2505**	**470**	High
Cold (strong)	2007-2008	12 months	-1,14	2087	52	Low
Cold (strong)	**2010-2012**	**22 months**	**-1,14**	**2560**	**526**	High
Warm (very strong)	2015-2016	19 months	**2,14**	1588	-446	Medium

Source. Author' elaboration based on NOAA data (September 30, 2023)

*Average precipitation was calculated by adding up all months that corresponded to anomalous conditions.

deficit of up to 900 mm in the rainy season of 1997. Interestingly, the El Niño of the 2015-2016 period does not seem to have had such a significant impact on rainfall, even though it has registered the maximum increase in marine temperatures in history.

Table 7. Classification of precipitation difference

Difference	Category
0-200mm	Low
201-400mm	Medium
401-600mm	High
601-800mm	Very high
> 801mm	Extreme

Source: own elaboration, 2023

The cold phase that occurred in the period 1973-1976 left an excess of more than 1300 mm of rainfall with respect to the general average of the rainfall record, thus being one of the rainiest periods in the history of the region.

Due to it is analyzed precipitation data, it is important to consider only the rainiest months (May, June, July, August, September, and October) to estimate correlations, to minimize the noise caused by values of zero or close to zero, occurring during the dry season. This should increase the correlation values, revealing a clearer connection with the indices.

As can be seen, by eliminating the driest months, it is possible to reduce the high concentration of values close to zero, which increases the linear relationship in almost all cases, in a significant way. Only the NAO index shows a low relationship, so that it can be said that the NAO index has almost no observable influence in the study area, considering the correlation criteria analyzed. The figure below summarizes the correlations analyzed for year-on-year precipitation.

The figure above shows more clearly the increase in the correlation between precipitation and most indices when the drier months are eliminated. The correlation is doubled in many cases; for example, going from an R-value of -0.12 to -0.3, and from 0.02 to 0.09 in R^2 in the case of ONI, being the one with the greatest increase. Under these conditions, the best-fit linear function goes from explaining 2% of the behavior of the data to 9%, according to the R^2 of the precipitation-ONI correlation.

It is also important to note that, when eliminating the driest months, the precipitation-SOI correlation is the second highest, going from a value of $r = 0.1$ to $r = 0.26$, and from values of $R^2 = 0.01$ to $R^2 = 0.07$. Therefore, it can be said that the indexes that measure the behavior of ENSO: ONI, MEIv2 and SOI, show small correlation with precipitation in San Ramón, with ENSO in the area. The CLLJ does not present remarkable correlations, and the influence of the NAO does not show any relationship with the rainfall in San Ramon. The indexes that measure climatological behavior in the Caribbean and North Atlantic: NAO and CLLJ, have also a small correlation.

Although in some studies Alfaro et all. (1999), which found that some oceanic indices strongly influence the onset of the rainy season, while others have no influence. Alfaro et all, 2001) mention the influence of the Pacific and Atlantic oceans (Amador et all, 2006), mentioned that the eastern Pacific Ocean influences atmospheric conditions.

Waylen et al (1996), causing an early southward migration of the Intertropical Convergence Zone (ITCS) and thus an early end of the rainy season over

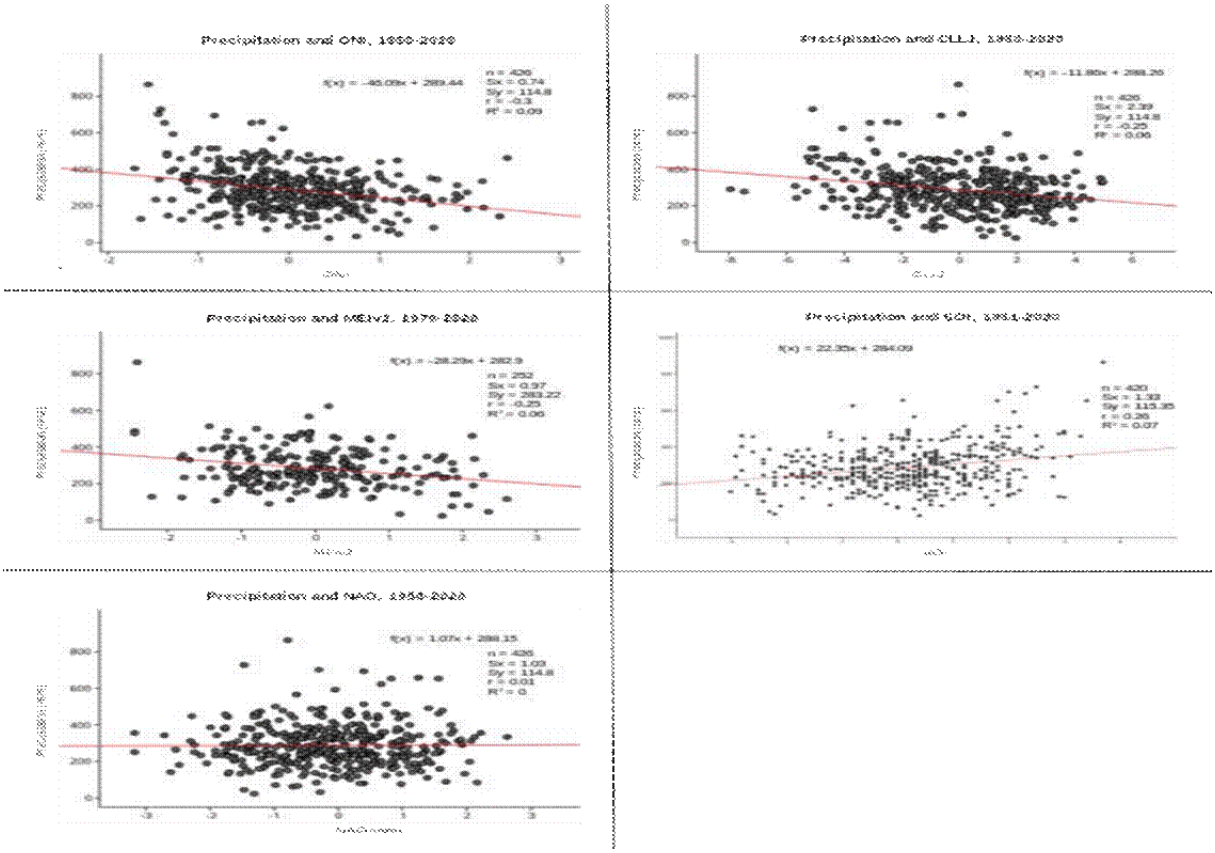

Source. Own elaboration based on the records of the San Ramón station and the NOAA indexes.

Figure 6. Relationships of precipitation with different indexes during the rainy season

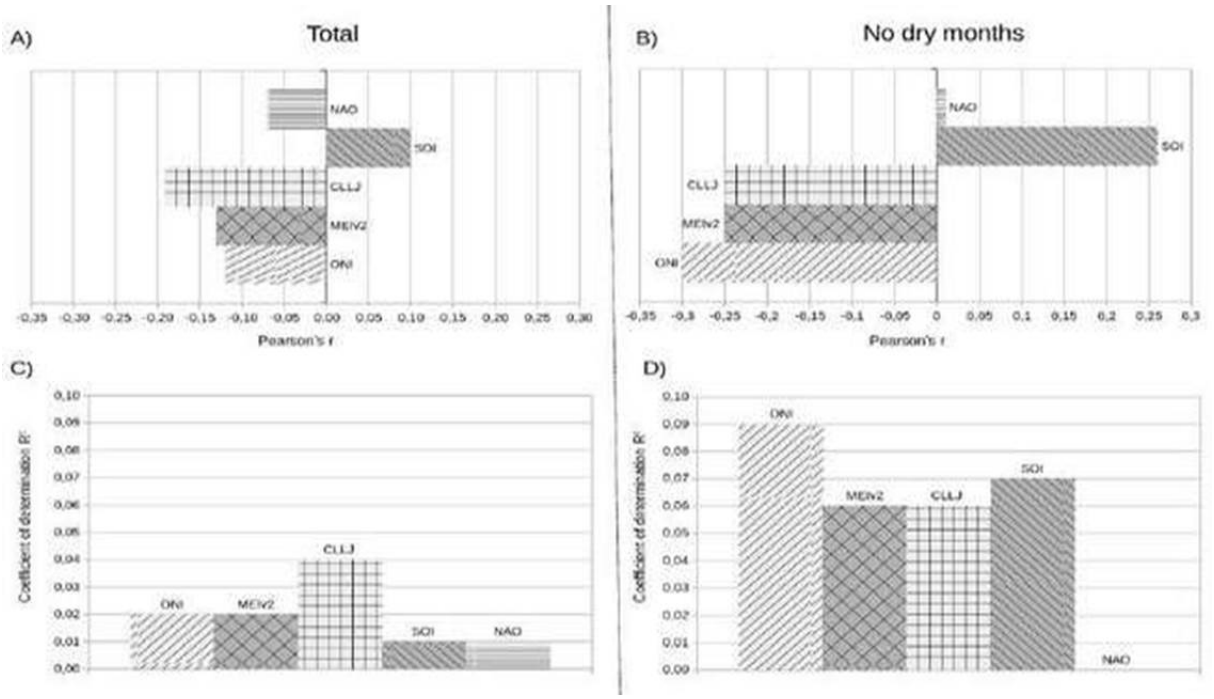

Source. Own elaboration based on the records of the San Ramón station and the NOAA indexes.

Figure 7. Correlation between precipitation and climate indexes, with and without dry months

Central America, which coincides with the dry conditions noted in the region by Ropelewski and Halpert (1987), during the months of Jul (0) to Oct (0). In this way, warm ENSO events would contribute negatively to the rainy season in Central America. Contrary situations, in the patterns of correlations between the physical variables described above, for cold ENSO events, were found by Hastenrath et al. (1987).

4. DISCUSSION AND CONCLUSIONS

It was established that rainfall in San Ramon tends to be above normal when La Niña conditions are present and below normal under El Niño (Waylen at all, 1996). Some applied indexes tend to have an adverse behavior, when they are negative values, increases the variables in the area under study, this can be seen when a regression is given in Figure 6, While oceanic indexes show a positive correlation with respect to rainfall in the San Ramon area.

The SOI index is shown as the only one with an increasing trend on the figure 6, giving a linear correlation r of 0.1, which implies that, at positive values of the index, there tends to be higher levels of precipitation. The different intensities of ENSO, and precipitation was correlated with the different oceanic-atmospheric indexes, showing a negative relationship in four of them and a positive relationship in only one. The NAO index shows a low regression, while the ONI, is showing negative values during La Niña (cold phase), producing above-average rainfall in the area under study. While during the El Niño event (warm phase) there have been decreases in precipitation (Waylen at all, 1996).

ENSO manifests itself in the tropical oceanic and atmosphere as a zonal seesaw between the eastern equatorial Pacific and Atlantic Oceans. The interaction between the two basins (oceans) takes place primarily through an anomalous Walker circulation, set up by the eastward shift of the convectively active region in the Pacific. This involves ascent over the eastern Pacific and descent over the equatorial Atlantic. An unusually warm water of the central Pacific is lower than average, it tends to be higher than average over the equatorial Atlantic, with the Caribbean constituting the boundary between negative and positive anomalies (Hastenrath et al.,1987; Waylen et all, 1996; Alfaro et all, 2001; IMN, 2018; Sheldon, 2019).

This seesaw pattern has a direct effect on convergence in the Caribbean basin. When is higher than average in the Atlantic, and lower than average in the eastern Pacific, the atmospheric flow at the surface is divergent over the Caribbean basin, along a southwest- to-northeast axis, with convergence onto the eastern Pacific ITCZ, to the west, and into the tropical North Atlantic, to the east. Hence the reduction of local moisture flux convergence.

In addition to the tropical “seesaw” in sea level pressure, the effect of ENSO is indirectly related to the North Atlantic, by a wave train pattern, in an alternance of high and low- pressure centers. This pattern above analyzes for the 2023 has changed because both oceans has gotten a warm sea surface temperature, which has conducted to has some cyclones in both oceans and several tropical waves coming from the Southeast in the Atlantic Ocean influencing the area in study (IMN, 2023).

5. ACKNOWLEDGEMENTS

We would like to thank Ricardo Prado G. for elaborating figures and tables. To the Vicerrectoría de Investigación and la Coordinación de Investigación, University of Costa Rica which was partially funded by Research Project 540-B8-052. To the anonymous reviewers for their valuable contributions to the research.

6. REFERENCES

Alfaro et all (1999). Análisis de las Anomalías en el inicio y el término de la estación lluviosa en Centroamérica y su relación con los océanos Pacífico y Atlántico Tropical**.** Top. Meteor. Oceanog., 6(1):1-13**.** IMN, Costa Rica.

Alfaro, E. (2000). Eventos cálidos y fríos en el Atlántico Tropical Norte. Atmósfera 13: 109- 119.

Alfaro, E.J. & O.G. Lizano. (2001). Algunas relaciones entre las zonas de surgencia del Pacífico Centroamericano y los océanos Pacífico y Atlántico tropicales. Rev. Biol. Trop. 49 (Suppl. 2): 185-193.

Alfaro E y Jorge Cortés. (2012). Atmospheric forcing of cool subsurface water events in Bahía Culebra, Gulf of Papagayo, Costa Rica. Rev. Biol. Tropical. vol.60 suppl.2 San José Apr.

Amador, J.A., E.J. Alfaro, O.G. Lizano & V. Magaña. (2006). Atmospheric forcing of the eastern tropical Pacific. A Review. *Prog. Oceanogr.* **69**: 101-142.

Amador, J. A., Rivera, E. R., Durán-Quesada, A. M., Mora, G., Sáenz, F., Calderón, B., & Mora, N. (2016). The easternmost tropical Pacific. Part I: A climate review. Revista de Biología Tropical, 64(Supplement 1), 1-22. https://doi.org/10.15517/rbt.v64i1.23407.

Bengtsson, L.; Rana, A. (2014). Long-term change of daily and multi-daily precipitation in southern Sweden. *Hydrol. Process. 28*, 2897-2911.

Boers et al., (2014). Prediction of extreme floods in the eastern Central Andes based on a complex network approach. National. 5:5199 | DOI: 10.1038/ncomms6199 | http://www.nature.com/nature communications.

Cerón, W.L.; Kayano, M.T.; Andreoli, R.V.; Avila-Diaz, A.; Ayes, I.; Freitas, E.D.; Martins, J.A.;

Souza, R.A.F. (2021). Recent intensification of extreme precipitation events in the La Plata Basin in Southern South America (1981-2018). *Atmos. Res. 249*, 105299. [**Google Scholar**] [**CrossRef**]

Doyle, M.E.; Saurral, I.; Barros, V.R. (2012). Trends in the distributions of aggregated monthly precipitation over the La Plata Basin. *Int. J. Climatol.*, *32*, 2149-2162. [**Google Scholar**] [**CrossRef**]

Du, H.; Xia, J.; Zeng, S.D.; She, D.X.; Liu, J.J. Variations, and statistical probability characteristic analysis of extreme precipitation events under climate in Haihe River Basin, China. *Hydrol. Process.* 2014, *28*, 913-925.

Endo, N.; Ailikun, B.; Yasunari, T. (2005). Trends in precipitation amounts and the number of rainy days and heavy rainfall events during summer in China from 1961 to 2000. *J. Meteorol. Soc. Japan*, *83*, 621-631. [**Google Scholar**] [**CrossRef**] [**Green Version**]

Frame, T.H., Methven, J., Roberts, N. M., Titley, H. A., 2015. Predictability of Frontal Waves and Cyclones. Weather and Forecasting, 30(5), 1291-1302.

Fowler, H.J.; Ali, H.; Allan, R.P.; Ban, N.; Barbero, R.; Berg, P.; Blenkinsop, S.; Cabi, N.S.; Chan, S.; Dale, M.; et al. (2021). Towards advancing scientific knowledge of climate change impacts on short-duration rainfall extremes. *Philos. Trans. R. Soc.*, *379*, 20190542.

Hyndman, R. J. (1995). The problem with Sturges rule for constructing histograms. Department of Economics & Business Statistics, Norash University. https://robjhyndman.com/papers/sturges.pdf

Instituto Meteorológico Nacional [IMN]. (2018). *El niño: fase cálida del ENOS*. ENOS. https://www.imn.ac.cr/documents/10179/37774/5-EL+NI%C3%91O_FASE_CALIDA_ENSO.pdf/0b8e55b1-c560-4fd7-aae2-710c95527702.

IMN (2023). Información dada por funcionarios del IMN en noticieros. Septiembre 2023.

Mclead (2022). Kendall Rank Correlation Mann-Kendall Trend Test. Version2.2.1

Mendenhall et al. (2010). Introducción a la Probabilidad y la estadística. CENGAGE. 13 Edición. México.

Mei, C.; Liu, J.; Chen, M.T.; Wang, H.; Li, M.; Yu, Y. (2018). Multi-decadal spatial and temporal changes of extreme precipitation patterns in northern China (Jing-Jin-Ji district, 1960-2013). *Quat. Int. 476*, 1-13.

Muñoz, E., Busalacchi, A.J., Nigam, S., Ruiz-Barradas, A., (2008). Winter and summer structure of the Caribbean low-level jet. J. Clim. 21 (6), 1260-1276. https://doi.org/10.1175/2007JCLI1855.1.

National Oceanographic and Atmospheric Administration [NOAA]. (30 de septiembre de 2023). *Oceanic Niño Index. Datasets useful for ENSO research*. https://psl.noaa.gov/enso/data.html

National Oceanographic and Atmospheric Administration [NOAA]. (2022c). Multivariate ENSO Index Version 2 (MEI.v2). https://psl.noaa.gov/enso/mei/

Palade D, D Pierce, D Cayan, A Gershunov, M Dettinger. (2014). The key role of dry days in changing regional climate and precipitation regimes. Scientific reports Nature.com

Quesada M y P. Waylen. (2012). Diferencias hidrológicas anuales y estacionales en regiones adyacentes: estudio de las subcuencas de los ríos Virilla y Grande de San Ramón, Costa Rica. Cuad. Geogr. Rev. Colombia. Geogr., Volumen 21, Número 2, p. 167 - 179, 2012. ISSN electrónico 2256-5442. ISSN impreso 0121-215X.

Quesada M.E. (2019). Precipitación acumulación en las tierras altas entre las secciones Tilarán y Central, Costa Rica**.** Physis Terrae. Vol. 1 No.1.

Quesada y Marsik (2014). Reacciones en la Precipitación ante oscilaciones oceánicas en sus temperaturas superficiales. Depresión Tectónica Central, Costa Rica. Papeles de Geografía. No. 59-60.

Ropelewski, C., and M. Halpert, 1987: Global and regional scale precipitation associated with El Nino/Southern Oscillation. Mon. Weather Rev, 115, 1606-1626..

Ropelewski, C., and M. Halpert, 1989: Precipitation patterns associated with the high index phase of the Southern Oscillation. J. Climate, 2, 268-284

Sheldon K. (2019). Climate Change in the Tropics: Ecological and Evolutionary Responses at Low Latitudes. Annual Review of Ecology, Evolution, and Systematics Vol. 50: 303- 333

Tao et al. (2016). Anthropogenic forcing on the Hadley circulation in CMIP5 simulations. Climate Dynamics. 63337-3350.

Varun Joshi and Kireet Kumar (2006). Extreme rainfall events and associated natural hazards in Alaknanda Valley, Indian Himalayan Region. https://www.researchgate.net/publication/225652390.

Vuille, M., Burns, S. J., Taylor, B. L., Cruz, F. W., Bird, B. W., Abbott, M. B., et al. (2012). A review of the South American monsoon history as recorded in stable isotopic proxies over the past two millennia. *Clim. Past* 8, 1309-1321. doi: 10.5.

Waylen, P., C. Caviedes, and M. Quesada, 1996: Interannual variability of monthly precipitation in Costa Rica. J. Climate, 9, 2606-2613..

Waylen, P., M. Quesada, and C. Caviedes, 1994: The effects of El Niño-Southern Oscillation on precipitation in San Jose, Costa Rica. Int. J. Climatol., 14, 559-568